Hindawi Publishing Corporation
International Journal of Photoenergy
Volume 2013, Article ID 729460, 8 pages
http://dx.doi.org/10.1155/2013/729460

Research Article

One-Step Synthesis of TiO_2/Perlite Composites by Flame Spray Pyrolysis and Their Photocatalytic Behavior

M. Giannouri,[1] Th. Kalampaliki,[1] N. Todorova,[1] T. Giannakopoulou,[1] N. Boukos,[1] D. Petrakis,[2] T. Vaimakis,[2] and C. Trapalis[1]

[1] *Institute of Advanced Materials, Physicochemical Processes, Nanotechnology and Microsystems, NCSR Demokritos, Agia Paraskevi, Attikis, 153 10 Athens, Greece*
[2] *Department of Chemistry, University of Ioannina, 451 10 Ioannina, Greece*

Correspondence should be addressed to C. Trapalis; trapalis@ims.demokritos.gr

Received 16 September 2013; Accepted 17 October 2013

Academic Editor: Jiaguo Yu

TiO_2/perlite composites were prepared via facile one-step flame spray pyrolysis (FSP) route. Titanium alkoxide (TIPO) and expanded perlite were used as Ti source and substrate, respectively. Precursor TIPO-ethanol solutions containing homogeneously dispersed perlite particles were processed through FSP setup at different experimental conditions regarding the gas flow and precursor supply rates. The structure, morphology, and the composition of the obtained powders were investigated. The porosity and the light absorbance of the TiO_2/perlite composites were examined and their photocatalytic activity in NO oxidation was evaluated. Commercial titania powder P25 was also FSP processed and investigated for comparison. The XRD analysis revealed that biphased titania with different anatase-rutile ratio and particles size 20–40 nm was synthesized onto the perlite which according to microscopy results was covered by neck-connected TiO_2 nanoparticles. The anatase-rutile interplay was also demonstrated by the Raman spectra where presence of Si-O-Ti vibrational modes was observed for some samples. The UV-Vis diffuse reflectance spectra of the TiO_2/perlite composites revealed up to 70% reflection that was connected to the presence of the gray perlite and superficial carbon. The best photocatalytic activity of the composites was connected to almost equal anatase-rutile ratio and possible synergetic effect of the two TiO_2 phases.

1. Introduction

The TiO_2 semiconductor is one of the most investigated materials during the last years. TiO_2 nanoparticles are used nowadays in an enormous spectrum of applications such as solar cells [1], gas sensors [2], photochromic devices [3], superhydrophilic surfaces [4] and photocatalysts [5]. The above applications are related to the three different crystalline phases of TiO_2, anatase, rutile, and brookite [6]. Both anatase and rutile crystal structures are commonly used as photocatalysts with anatase showing a greater activity for most photocatalytic processes. This is attributed to anatase's slightly higher Fermi level, its lower capacity to adsorb oxygen, and its higher degree of hydroxylation [7, 8]. There are also studies which claim that a synergetic effect occurs and a mixture of anatase and rutile is more active than pure anatase [9]. The enhanced activity arises from the increased efficiency of the electron-hole separation due to the multiphase nature of the photocatalyst [10].

Various procedures are established for producing photocatalyst particles such as chemical vapour deposition [11], precipitation [12, 13], sol-gel methods [14], and hydrothermal synthesis [15–18].

The last one is a fast, profitable, and flexible process for the production of a wide variety of different nanoparticles [19]. In this process, flame is being used to drive chemical reactions of precursor compounds [20–26], resulting in the formation of clusters, which grow to nanometer-sized products by coagulation and sintering. In particular, TiO_2 or TiO_2-containing composite systems were studied by flame spray pyrolysis such as $(TiO_2)_x(Al_2O_3)_{1-x}$ [20], Au/TiO_2 [21],

Pt/TiO_2, Fe/TiO_2 [22], V_2O_5/TiO_2 [23], Cr/TiO_2 [24], Ag/TiO_2 [25], and $SiO_2/V_2O_5/WO_3/TiO_2$ systems [26].

There are several works investigating deposition of TiO_2 nanoparticles on various surfaces such as polymeric matrices [27], graphene oxide [28], carbon fibers [29], clays [30], and layered double hydroxide LDH [31–33]. Systems of nanosized TiO_2 with highly adsorptive supports enhance the performance of the photocatalysts due to larger specific area, porosity, and higher adsorption capacity in comparison to the bare TiO_2. Support limits the aggregation of TiO_2 nanoparticles, induces the microporosity into the materials [31], and contributes to the efficient spatial separation between the photogenerated electrons and holes. Glassy substrates were also used for deposition of TiO_2 photocatalysts [34–37]. Such a glassy substrate is the perlite which is a natural amorphous material widely used in construction and industry. The use of natural perlite in blended cement production was investigated and the results revealed that perlite possesses sufficient pozzolanic characteristics [38]. Its average chemical composition is approximately 75% SiO_2 with oxides of Al (14.8%), K (4.8%), Na (2.9%), Ca (0.9%), Mg (0.1%), Fe_2O_3 (1.5%), and water (4.0%) [39]. Crude perlite particles expand after heating to 870°C due to the presence of water and form innumerable sealed glassy cells in a manner similar to popcorn. These account for the excellent insulating properties and light weight of the expanded perlite. Being highly porous and chemically inert media, perlite granules can act as a good adsorbent. Therefore, expanded perlite can be selected as substrate for TiO_2 particles.

TiO_2/perlite composites prepared by various experimental methods were investigated aiming at enhanced photocatalytic activity in water and air decontamination. Thus, the TiO_2-coated perlite granules were prepared using sol-gel method and tested for photocatalytic purification of furfural polluted waste water [40]. Also, TiO_2 (Evonik-Degussa P25) immobilized on different supports (perlite granules, glass plates, and steel fiber) by sol-gel and investigated their photocatalytic oxidation of phenol [41]. The preceding works on TiO_2/perlite composite materials used mainly wet chemistry to immobilize the photocatalyst onto the substrate. To the best of our knowledge, there is only one report on preparation of Ag-coated perlite by the spray pyrolysis method in order to obtain a catalyst for ozone decomposition using a cheap natural glass as substrate [42].

In this paper we present for the first time the one-step synthesis of the TiO_2/perlite composites by flame spray pyrolysis (FSP) processing. The structural and the morphological properties of the prepared materials as well as their photocatalytic performance in air pollutants oxidation are examined.

2. Experimental

2.1. Precursor Materials. The expanded perlite was provided by S&B Industrial Minerals S.A. to be used as a support for deposition of TiO_2 nanoparticles. Perlite was ground in a planetary mill for 2 h in order for fine granules to be obtained.

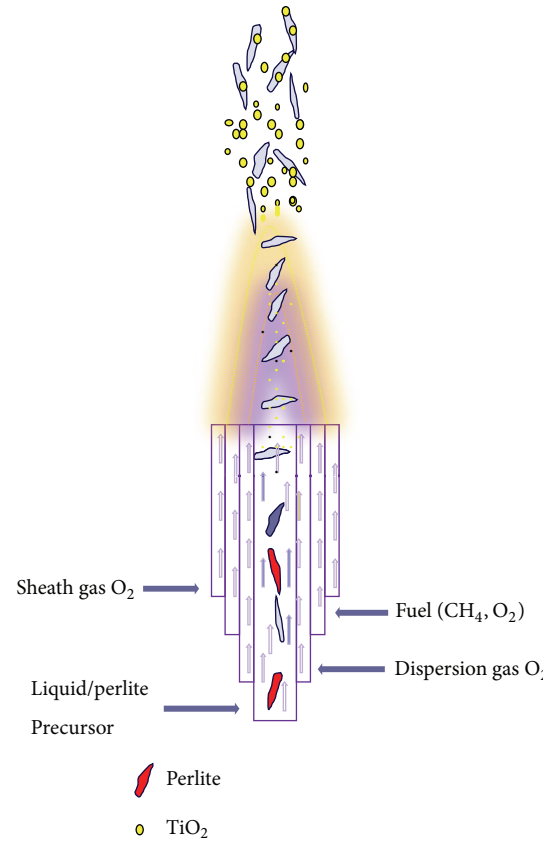

Figure 1: Schematic of the flame spray pyrolysis device. During spray procedure and after evaporation and combustion of precursor, TiO_2 nanoparticles are formed on perlite substrate.

The TiO_2/perlite composite materials were prepared as follows. Initially, 5 mL titanium isopropoxide (TIPO), Aldrich 97%, was dissolved in 40 mL ethanol, Carlo Erba, and stirred for 30 min. Then, 5 g perlite was added and the dispersion was stirred for 60 min. The mixture was further homogenized using an ultrasound tip sonicator (Hielscher UIP 1000 hd). Total energy input of 1 Wh was applied for sonication time for 2 min. Finally, the slurry was diluted with ethanol to receive 100 mL suspension and the liquid obtained was nominated as precursor solution (PS). The prepared PS was ready to be processed through the flame spray pyrolysis system. It should be noted that water was not used in order to avoid hydrolysis.

2.2. Flame Spray Pyrolysis Device. A homemade FSP setup was used to synthesize TiO_2/perlite composites. In Figure 1 the schematic of the experimental set-up is shown. The FSP reactor consisted of four stainless steel concentric tubes. The PS was fed by a syringe pump (Inotec, IER-560) through the innest capillary tube (i.d. 0.8 mm). Oxygen was used as dispersion gas fed through the surrounding annulus (i.d. 2.5 mm, o.d. 3.0 mm) with a pressure drop of 1.5 bar and a rate in the range of 10–20 L min^{-1}.

The resulting spray was ignited by a circular premixed flame (i.d. 17.0 mm, o.d. 19.7 mm) of CH_4 (1.5 L min^{-1}) and O_2 (3.2 L min^{-1}). An additional O_2 sheath flow (20–40 L min^{-1})

Table 1: Anatase (W_A%) and rutile (W_R%) compositions, crystallite sizes (d_A and d_R) under different sheath, dispersion oxygen fractions, and syringe pump flow rates.

Samples	Dispersion flow rates L min^{-1}	Sheath flow rates L min^{-1}	Syringe pump rates mL min^{-1}	d_A nm	d_R nm	W_A (%)	W_R (%)
P25				20	27	85	15
FSPA	14.0	20.0	12.0	24	30	48	52
FSPB	19.0	28.9	10.0	29	42	72	28
FSPC	17.3	38.8	12.0	27	31	70	30
FSPD	10.9	55.0	10.0	30	28	55	45

for complete combustion of the precursor was supplied through a sinter metal ring (i.d. 30 mm, o.d. 38 mm). In this paper, the total O_2 flow rate represents the sum of dispersion and sheath O_2 supply. The gas flow rates were regulated by calibrated mass flow controllers (Bronkhorst EL-Flow). The PS was processed through the FSP and the resulting powders were collected on glass microfiber filters (Whatman GF/D, 257 mm diameter) with the aid of a vacuum pump. Different TiO_2/perlite samples were prepared by variation of the experimental conditions, namely, the gas flow rates (dispersion and sheath) and the syringe pump rate for the PS supply. Table 1 summarizes the above parameters used during the FSP process as well as the fraction of anatase and rutile phases of the flame made samples.

2.3. Characterization of TiO_2/Perlite Composites. The XRD patterns of the samples were obtained by X-ray diffractometer (SIEMENS D500) with secondary graphite monochromator and CuKa radiation operating in Bragg-Brentano geometry. The measured 2θ range between 10° and 90° was scanned in steps of 0.03°/2 s. The accelerating voltage and applied current were 40 kV and 35 mA, correspondingly. The crystalline phases were identified with reference to the PDF cards of the International Centre for Diffraction Data. The average crystallite sizes of the anatase and rutile phases were determined from the intensities of the primary peaks of anatase (101) reflection at $2\theta_B = 25.3°$ and rutile (110) reflection $2\theta_B = 27.5°$ using the Scherrer relation [43] as follows:

$$d\,(\text{nm}) = \frac{0.89 \times \lambda}{B\,(\text{rad}) \cos\theta_{\text{B}}}, \tag{1}$$

where $\lambda = 0.15418$ nm is the X-ray wavelength, B (rad) is the full width at the half maximum of the diffraction peak, and θ_{B} is the Bragg angle.

Since only the anatase and rutile phases are present in the examined TiO_2/perlite composites, the weight content of these phases was derived from the area of the corresponding peak after the background substraction using (2) [44] as follows:

$$W_R\,(\%) = \frac{S_R}{0.886 \times S_A + S_R},$$
$$W_A\,(\%) = 100 - W_R\,(\%), \tag{2}$$

where S_R and S_A are the surfaces of the primary rutile (110) and anatase (101) peaks, correspondingly.

Table 2: Measured BET SSA of the TiO_2/perlite composites and calculated SSA of their TiO_2 component with respect to the total oxygen flow rate.

Samples	SSA_{COMP} m^2/gr	SSA_{TiO_2} m^2/gr	O_2 flow rate L min^{-1}
FSPA	20.0	55.6	34.0
FSPB	20.2	48.4	47.9
FSPC	19.4	53.4	56.1
FSPD	12.8	51.1	66.0

The specific surface areas (SSA) of the powders were determined via Brunauer-Emmett-Teller (BET) method. Standard device Sorptomatic 1990 FISONS was used for the nitrogen adsorption/desorption measurements at 77°K. All the samples were degassed at 453°K for 12 h. Assuming spherical and unagglomerated particles, the SSA of the TiO_2 nanoparticles (SSA_{TiO_2}) was calculated from the average particle diameter estimated by XRD spectra, $d^{XRD}{}_{A(R)}$, and the weighted density of the particles $\rho_{A(R)}$ (anatase: $\rho_A = 3.84$ gr/cm^3, rutile: $\rho_R = 4.26$ gr/cm^3) by (3) as follows:

$$\text{SSA}_{A(R)} = \frac{6}{\left(\rho_{A(R)} \times d^{\text{XRD}}{}_{A(R)}\right)}. \tag{3}$$

The SSA_{TiO_2} was calculated taking into account the mass fraction of anatase and rutile phases. The BET measured SSA of TiO_2/perlite composites (SSA_{COMP}) and the calculated SSA_{TiO_2} are presented in Table 2.

The structural properties of the prepared composite materials were examined by Raman spectroscopy. The Raman spectra were measured with an inVia Raman microscope (Renishaw) using the 514.5 nm line of Ar+ laser emission with a resolution of 1.1 cm^{-1}. The laser power was 50 mW as an output and Raman emission signal at each measurement point was accumulated for 20 s for all samples.

UV-Vis diffuse reflectance of the powders in the wavelength range 350–800 nm as obtained using UV-2100 Shimadzu instrument. The measurements were performed using $BaSO_4$ etalon as a baseline.

The morphology of the powders was observed using scanning electron microscopy (SEM). An FEI Inspect microscope with tungsten filament operating at 25 kV was employed. In order to improve the surface conductivity of the samples standard gold deposition was applied through vacuum evaporation.

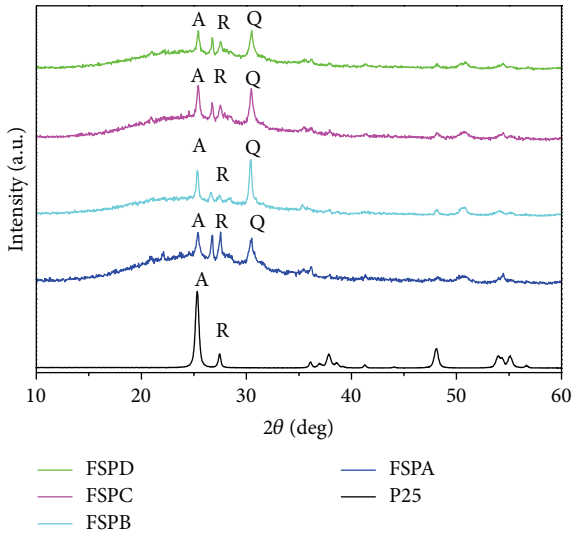

Figure 2: XRD patterns of TiO_2/perlite correspond to the (101) reflection of the anatase and to the (110) of the rutile. For comparison, the XRD pattern of Degussa P25 is presented.

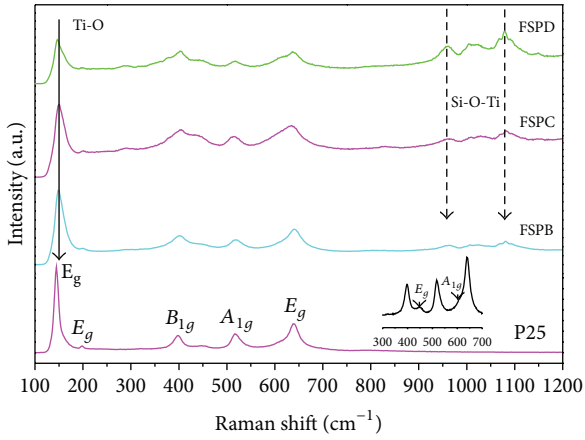

Figure 3: Raman spectra of samples P25, FSPB, FSPC, and FSPD.

The samples were also investigated using transmission electron microscopy (TEM). An FEI CM20 microscope operated at 200 kV was used. The samples for TEM observation were prepared as follows. Small amounts of the studied photocatalysts were dispersed in ethanol and the suspensions were treated in ultrasonic bath for 10 min. Then, a drop of the dilute suspension was placed on a carbon-coated grid and was allowed to dry by evaporation at ambient temperature.

Nitric oxide (NO) was chosen as representative airborne pollutant due to its potential health risks and ability to generate photochemical smog. The photocatalytic oxidation of NO by the prepared TiO_2/perlite composite materials was investigated employing standard procedure based on ISO/DIS 22197-1 [45]. The experimental set-up, the procedures of specimens' preparation, and photocatalytic activity measurement are described elsewhere [46–49]. Briefly, the samples were placed in a flow-type photoreactor where model air containing 1 ppm NO was issued. Flow rate of 3 L/min

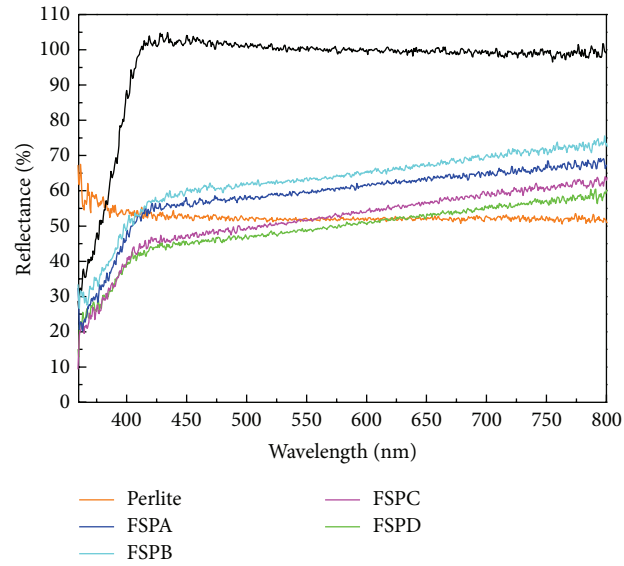

Figure 4: Diffuse reflectance spectra of TiO_2/perlite samples.

and relative humidity of 50% were retained during the experiment. UV-A light illumination with intensity 10 W/m^2 for 90 min was applied. The concentrations of the NO, NO_2, and NO_x (NO_x = NO − NO_2) were monitored in dark and under illumination. The photocatalytic activity of the samples was expressed by the calculated photonic efficiency ζ (mole/einstein) in NO and NO_2 oxidation as well as in NO_x removal for the entire illumination period.

3. Results and Discussion

The measured XRD patterns of the prepared materials are shown in Figure 2. It can be observed that the samples were crystallized in the form of anatase and rutile. The position and the relative intensities of the peaks are consistent with the anatase TiO_2 JCPDS card number 21-1272 and rutile TiO_2 JCPDS card number 21-1276. The average crystallite size obtained from the most intensive diffraction peaks (101) and (110) at $2\theta = 25.28^\circ$ and $2\theta = 27.45^\circ$ ranged between 20 and 30 nm for anatase phase and 27 and42 nm for rutile phase, respectively (Table 1). Also, a broadened bump in the 2θ range from 20° to 35° was observed originating from the amorphous nature of perlite. In the same time, the diffraction peaks (100), (101) and (110) were attributed to evident partial crystallization of the perlite during the flame processing procedure. The broadened part and quartz peaks are absent in the sample FSPA, which consist of P25 Degussa only. Finally, the interplay between the anatase and rutile phases in the composites (Table 1) is influenced by the PS and total O_2 flow rates [50], but the clear tendency in its behavior cannot be determined from our experiments.

In previous papers, it was demonstrated that the SSA of the particles decreased with the increase of the precursor flow rate [51, 52] as well as with the increase of the oxygen flow rate [23]. Higher precursor flow rate provokes higher frequency of the particle collision and sintering due to higher

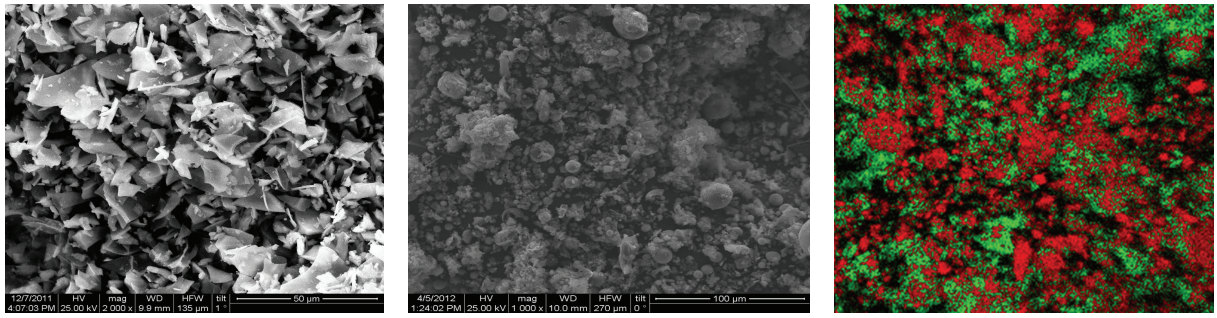

(a) (b) (c)

Figure 5: Scanning electron microscopy (SEM) micrographs of pure perlite (a), composite TiO_2/perlite (b), and elemental mapping for the FSPD sample using energy dispersive spectroscopy (c). Red colour corresponds to Si and green to Ti.

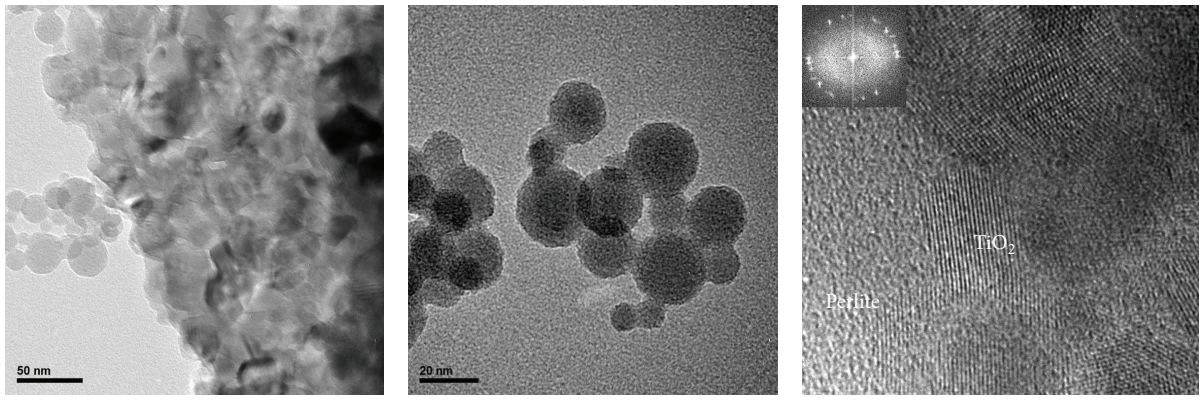

(a) (b) (c)

Figure 6: TEM micrographs of the composite TiO_2/Perlite (a), TiO_2 nanoparticles (b), and HRTEM image of TiO_2/Perlite (c).

concentration of the forming powder in the flame. Also, higher oxygen flow rate leads to higher flame temperature encountered by the particles. As a result, the enlargement of particle size and reduction of their SSA were observed in both cases.

The BET measured SSA of the composites (SSA_{COMP}) and the calculated SSA of TiO_2 particles (SSA_{TiO_2}) as well as total oxygen flow rate used in our experiments are given in Table 2. It can be perceived that the SSA_{COMP} is lower than SSA_{TiO_2}. This can be explained by mixing of photocatalytically active TiO_2 component with porous but lower SSA perlite substrate. In addition, given that the precursor flow rate does not vary considerably, it seems that both SSA values decrease with the increase of the oxygen flow rate. This correlates with the literature results mentioned above.

The Raman spectra of the investigated composites as well as of the reference P25 sample are given in Figure 3.

The presence of the two anatase and rutile phases demonstrated by the XRD results above and their alteration can be observed also for the prepared composites. Thus, the Raman lines of the anatase phase [53] at 144 cm^{-1} (E_g mode), 197 cm^{-1} (E_g mode), 399 cm^{-1} (B_{1g} mode), 515 cm^{-1} (A_{1g} mode), and 639 cm^{-1} (E_g mode) can be observed in all the samples. Additionally, a weak peak at 450 cm^{-1} and a small shoulder around at 610 cm^{-1} were also found in the reference sample (Figure 3-inset). Both peaks correspond to the E_g and A_{1g} modes of the rutile phase, respectively [54]. These rutile peaks were changed in the spectra of the TiO_2/perlite composites (samples FSPA, FSPB, and FSPD). More specifically, the shoulder at 610 cm^{-1} disappeared and the weak peak at 450 cm^{-1} caused a broadening of the anatase peak around 399 cm^{-1}.

It can be also observed that the lowest E_g anatase mode near 144 cm^{-1} is shifted to higher wavenumbers in the binary TiO_2/perlite systems (samples FSPB, FSPC, and FSPD) in comparison to the bare TiO_2 nanoparticles (reference P25). The blue shift can be attributed to compressive stresses appeared in the samples during the flame processing procedure [55]. This procedure is very abrupt and can evoke stresses in the flame-made nanoparticles produced using alkoxide precursor in comparison to the sample P25.

In addition, the peaks at 950 cm^{-1} and 1080 cm^{-1} related to the vibrational modes of Si-O-Ti [56] were observed for the samples FSPB, FSPC, and FSPD. This is an indication of the bond formation between TiO_2 photocatalysts and perlite substrate during the FSP processing.

The UV-Vis diffuse reflectance spectra for the prepared photocatalysts are given in Figure 4. It can be observed that

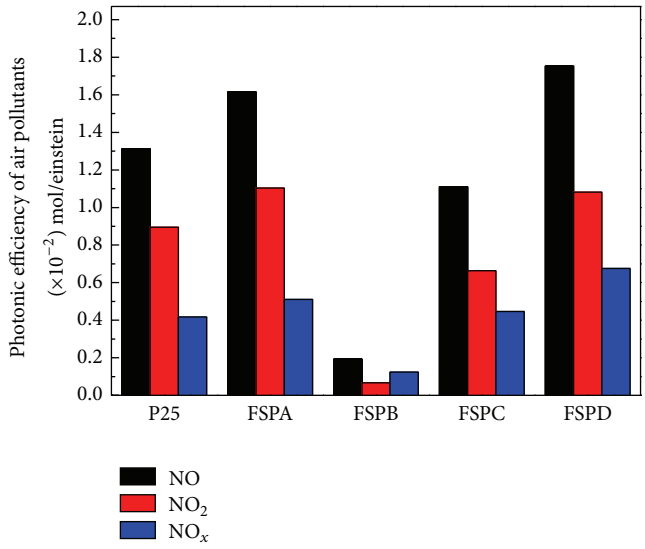

Figure 7: Photonic efficiencies in NO oxidation, NO_2 formation, and overall NO_x removal of the TiO_2/perlite composites.

the reflectance was high only for the reference sample P25. The bare perlite and all the TiO_2/perlite composites had a reflectance not higher than 70%. It was attributed to the presence of gray colored perlite in the prepared composites and probably to a large amount of residual carbon from the precursor and gas combustion.

The SEM images of the pure perlite and the perlite with immobilized titania nanoparticles are shown in Figures 5(a) and 5(b), respectively. It can be seen that bare perlite has a flake-like form. In the FSP composites, the flakes become rounded and are covered with TiO_2 agglomerates. This change in the perlite morphology is attributed to the high temperature FSP processing. The elemental mapping analysis presented in Figures 5(b) and 5(c) reveals that titania (Ti green colour) is homogenously dispersed on the surface of perlite (Si red colour).

Further morphological and structural characterization of the samples was carried out using TEM. As can be seen in Figure 6(a) the perlite flakes are almost entirely covered by TiO_2 nanoparticles that appear as an aggregation of small spherical neck-connected particles. It is suggested that these particle aggregations were created from large precursor solution droplets originated from 800 μm nozzle diameter. The precursor rapid hydrolysis accompanied with droplets' abrupt shrinkage, during their passage through the flame zone, results in the formation of neck-connected spherical TiO_2 nanoparticles, as shown in Figure 6(b). Their mean size is about 20 nm in agreement with XRD results.

A typical HRTEM image of the TiO_2 nanocrystals on the perlite substrate is presented in Figure 6(c). It is evident that each nanoparticle is single crystalline. The lattice fringes shown in the HRTEM image correspond to the rutile and anatase crystal structure with d-spacing $d = 0.325$ nm and $d = 0.352$ nm, respectively. This result is further confirmed by the fast Fourier transform of the HRTEM image shown as inset in Figure 6(c).

The calculated photonic efficiencies of the investigated samples are presented in Figure 7. The calculated values for the commercial Evonik-Degussa P25 are also given for comparison. It can be seen that the FSPA and FSPD TiO_2/perlite composite samples exhibited improved photocatalytic activity in comparison to P25. In these samples, the anatase and rutile phase as well as TiO_2 are almost equal according to the XRD results.

Although the anatase is considered a more superior photocatalyst than rutile, the better photocatalytic performance of these composites can be related to possible synergistic effect between the two titania phases. Below is given a simple interpretation of this effect. Because of the higher position of the anatase's conduction band edge relative to that of rutile, transfer of the photogenerated electrons from the anatase to rutile takes place. This leads to reduction of the electron-hole recombination rate and as a result to enhancement of the photocatalytic activity of the composite material. Furthermore, the observed enhanced photoactivity of the TiO_2/perlite system can be also attributed to the presence of semitransparent porous perlite substrate that facilitates the dispersion of the TiO_2 particles as well as the penetration of UV-irradiation into the depth of the material [52, 57].

4. Conclusions

TiO_2/perlite composites were synthesized with the help of a homemade FSP reactor and using milled perlite flakes dispersed in TIPO and ethanol as precursor solution. The obtained TiO_2 consisted of interconnected spherical nanoparticles homogenously distributed on perlite flakes. The XRD analysis showed that titania crystallized in the form of anatase and rutile with nanoparticles' size ranging from 20 to 40 nm. Raman microscopy revealed attachment of titania nanoparticles onto perlite substrate via formation of the Si-O-Ti bond. The SSA of the TiO_2/perlite composites decrease with the increase of the oxygen flow rate. Although the SSA of the TiO_2/perlite composites was lower than that of P25 sample, their photocatalytic activity in NO oxidation was comparable and even higher for some of them. This result was attributed to the presence of perlite glassy substrate that facilitates photocatalyst dispersion as well as to the synergistic effect between two crystalline phases.

Acknowledgment

This work was partially supported by the General Secretariat for Research and Technology of Greece under the projects 09SYN-42-925-ARISTON and 12SLO ET36 62.

References

[1] B. O'Regan and M. Grätzel, "A low-cost, high-efficiency solar cell based on dye-sensitized colloidal TiO_2 films," *Nature*, vol. 353, no. 6346, pp. 737–740, 1991.

[2] M. J. Madou and S. R. Morrison, *Chemical Sensing with Solid State Devices*, Academic Press, Harcourt Brace Jovanovich Publisher, Boston, Mass, USA, 1987.

[3] M. Biancardo, R. Argazzi, and C. A. Bignozzi, "Solid-state photochromic device based on nanocrystalline TiO_2 functionalized with electron donor-acceptor species," *Inorganic Chemistry*, vol. 44, no. 26, pp. 9619–9621, 2005.

[4] R. Wang, K. Hashimoto, A. Fujishima et al., "Light-induced amphiphilic surfaces," *Nature*, vol. 388, no. 6641, pp. 431–432, 1997.

[5] M. R. Hoffmann, S. T. Martin, W. Choi, and D. W. Bahnemann, "Environmental applications of semiconductor photocatalysis," *Chemical Reviews*, vol. 95, no. 1, pp. 69–96, 1995.

[6] J. F. Banfield and H. Zhang, "Nanoparticles in the environment," *Reviews in Mineralogy and Geochemistry*, vol. 44, pp. 1–58, 2001.

[7] A. L. Linsebigler, G. Lu, and J. T. Yates Jr., "Photocatalysis on TiO_2 surfaces: principles, mechanisms, and selected results," *Chemical Reviews*, vol. 95, no. 3, pp. 735–758, 1995.

[8] K. Tanaka, M. F. V. Capule, and T. Hisanaga, "Effect of crystallinity of TiO_2 on its photocatalytic action," *Chemical Physics Letters*, vol. 187, no. 1-2, pp. 73–76, 1991.

[9] R. I. Bickley, T. Gonzalez-Carreno, J. S. Lees, L. Palmisano, and R. J. D. Tilley, "A structural investigation of titanium dioxide photocatalysts," *Journal of Solid State Chemistry*, vol. 92, no. 1, pp. 178–190, 1991.

[10] H. Gerischer and A. Heller, "Photocatalytic oxidation of organic molecules at TiO_2 particles by sunlight in aerated water," *Journal of the Electrochemical Society*, vol. 139, no. 1, pp. 113–118, 1992.

[11] K. Okuyama, Y. Kousaka, N. Tohge et al., "Production of ultrafine metal oxide aerosol particles by thermal decomposition of metalalkoxide vapors," *AIChE Journal*, vol. 32, no. 12, pp. 2010–2019, 1986.

[12] K. Palmisano, V. Augugliaro, A. Sclafani, and M. Schiavello, "Activity of chromium-ion-doped titania for the dinitrogen photoreduction to ammonia and for the phenol photodegradation," *Journal of physical chemistry*, vol. 92, no. 23, pp. 6710–6713, 1988.

[13] W. Choi, A. Termin, and M. R. Hoffmann, "The role of metal ion dopants in quantum-sized TiO_2: correlation between photoreactivity and charge carrier recombination dynamics," *Journal of Physical Chemistry*, vol. 98, no. 51, pp. 13669–13679, 1994.

[14] G. P. Fotou, S. Vemury, and S. E. Pratsinis, "Synthesis and evaluation of titania powders for photodestruction of phenol," *Chemical Engineering Science*, vol. 49, no. 24, pp. 4939–4948, 1994.

[15] S. Liu, J. Yu, and M. Jaroniec, "Tunable photocatalytic selectivity of hollow TiO_2 microspheres composed of anatase polyhedra with exposed 001 facets," *Journal of the American Chemical Society*, vol. 132, no. 34, pp. 11914–11916, 2010.

[16] J. Yu, W. Liu, and H. Yu, "A one-pot approach to hierarchically nanoporous titania hollow microspheres with high photocatalytic activity," *Crystal Growth and Design*, vol. 8, no. 3, pp. 930–934, 2008.

[17] K. Cheng, W. Sun, H. Y. Ying Jiang, J. Liu, and J. Lin, "Sonochemical deposition of Au nanoparticles on different facets-dominated anatase TiO_2 single crystals and resulting photocatalytic performance," *Journal of Physical Chemistry C*, vol. 117, no. 28, pp. 14600–146007, 2013.

[18] M. V. Sofianou, V. Psycharis, N. Boukos et al., "Tuning the photocatalytic selectivity of TiO_2 anatase nanoplates by altering the exposed crystal facets content," *Applied Catalysis B*, vol. 142, pp. 761–768, 2013.

[19] S. E. Pratsinis, "Flame aerosol synthesis of ceramic powders," *Progress in Energy and Combustion Science*, vol. 24, no. 3, pp. 197–219, 1998.

[20] S. Kim, J. J. Gislason, R. W. Morton, X. Q. Pan, H. P. Sun, and R. M. Laine, "Liquid-feed flame spray pyrolysis of nanopowders in the alumina-titania system," *Chemistry of Materials*, vol. 16, no. 12, pp. 2336–2343, 2004.

[21] G. L. Chiarello, E. Selli, and L. Forni, "Photocatalytic hydrogen production over flame spray pyrolysis-synthesised TiO_2 and Au/TiO_2," *Applied Catalysis B*, vol. 84, no. 1-2, pp. 332–339, 2008.

[22] W. Y. Teoh, L. Mädler, D. Beydoun, S. E. Pratsinis, and R. Amal, "Direct (one-step) synthesis of TiO_2 and Pt/TiO_2 nanoparticles for photocatalytic mineralisation of sucrose," *Chemical Engineering Science*, vol. 60, no. 21, pp. 5852–5861, 2005.

[23] S. Y. Dhumal, T. L. Daulton, J. Jiang, B. Khomami, and P. Biswas, "Synthesis of visible light-active nanostructured TiO_x ($x < 2$) photocatalysts in a flame aerosol reactor," *Applied Catalysis B*, vol. 86, no. 3-4, pp. 145–151, 2009.

[24] K. A. Michalow, E. H. Otal, D. Burnat et al., "Flame-made visible light active TiO_2:Cr photocatalysts: correlation between structural, optical and photocatalytic properties," *Catalysis Today*, vol. 209, pp. 47–53, 2013.

[25] C. Gunawan, W. Y. Teoh, C. P. Marquis, J. Lifia, and R. Amal, "Reversible antimicrobial photoswitching in nanosilver," *Small*, vol. 5, no. 3, pp. 341–344, 2009.

[26] R. Jossen, M. C. Heine, S. E. Pratsinis, S. M. Augustine, and M. K. Akhtar, "Thermal stability and catalytic activity of flame-made silica-vanadia-tungsten oxide-titania," *Applied Catalysis B*, vol. 69, no. 3-4, pp. 181–188, 2007.

[27] B. Sánchez, J. M. Coronado, R. Candal et al., "Preparation of TiO_2 coatings on PET monoliths for the photocatalytic elimination of trichloroethylene in the gas phase," *Applied Catalysis B*, vol. 66, no. 3-4, pp. 295–301, 2006.

[28] L.-W. Zhang, H.-B. Fu, and Y.-F. Zhu, "Efficient TiO_2 photocatalysts from surface hybridization of TiO_2 particles with graphite-like carbon," *Advanced Functional Materials*, vol. 18, no. 15, pp. 2180–2189, 2008.

[29] N. Keller, G. Rebmann, E. Barraud, O. Zahraa, and V. Keller, "Macroscopic carbon nanofibers for use as photocatalyst support," *Catalysis Today*, vol. 101, no. 3-4, pp. 323–329, 2005.

[30] P. Aranda, R. Kun, M. A. Martín-Luengo, S. Letaïef, I. Dékány, and E. Ruiz-Hitzky, "Titania-sepiolite nanocomposites prepared by a surfactant templating colloidal route," *Chemistry of Materials*, vol. 20, no. 1, pp. 84–91, 2008.

[31] Y. Lee, J. H. Choi, H. J. Jeon, K. M. Choi, J. W. Lee, and J. K. Kang, "Titanium-embedded layered double hydroxides as highly efficient water oxidation photocatalysts under visible light," *Energy and Environmental Science*, vol. 4, no. 3, pp. 914–920, 2011.

[32] S. Pausova, J. Krysa, J. Jirkovsky, G. Mailhot, and V. Prevot, "Photocatalytic behavior of nanosized TiO_2 immobilized on layered double hydroxides by delamination/restacking process," *Environmental Science and Pollution Research*, vol. 19, pp. 3709–3718, 2012.

[33] R. Lu, X. Xu, J. Chang, Y. Zhu, S. Xu, and F. Zhang, "Improvement of photocatalytic activity of TiO_2 nanoparticles on selectively reconstructed layered double hydroxide," *Applied Catalysis B*, vol. 111-112, pp. 389–396, 2012.

[34] M. H. Habibi and M. Zendehdel, "Synthesis and characterization of titania nanoparticles on the surface of microporous perlite using sol-gel method: influence of titania precursor

on characteristics," *Journal of Inorganic and Organometallic Polymers and Materials*, vol. 21, no. 3, pp. 634–639, 2011.

[35] J. Matos, J. Laine, J.-M. Herrmann, D. Uzcategui, and J. L. Brito, "Influence of activated carbon upon titania on aqueous photocatalytic consecutive runs of phenol photodegradation," *Applied Catalysis B*, vol. 70, no. 1–4, pp. 461–469, 2007.

[36] J. Matos, J. Laine, and J.-M. Herrmann, "Effect of the type of activated carbons on the photocatalytic degradation of aqueous organic pollutants by UV-irradiated titania," *Journal of Catalysis*, vol. 200, no. 1, pp. 10–20, 2001.

[37] A. Fernandez, G. Lassaletta, V. M. Jimenez et al., "Preparation and characterization of TiO_2 photocatalysts supported on various rigid supports (glass, quartz and stainless steel). Comparative studies of photocatalytic activity in water purification," *Applied Catalysis B*, vol. 7, no. 1-2, pp. 49–63, 1995.

[38] T. K. Erdem, Ç. Meral, M. Tokyay, and T. Y. Erdoğan, "Use of perlite as a pozzolanic addition in producing blended cements," *Cement and Concrete Composites*, vol. 29, no. 1, pp. 13–21, 2007.

[39] M. Singh and M. Garg, "Perlite-based building materials—a review of current applications," *Construction and Building Materials*, vol. 5, no. 2, pp. 75–81, 1991.

[40] M. Faramarzpour, M. Vossoughi, and M. Borghei, "Photocatalytic degradation of furfural by titania nanoparticles in a floating-bed photoreactor," *Chemical Engineering Journal*, vol. 146, no. 1, pp. 79–85, 2009.

[41] S. N. Hosseini, S. M. Borghei, M. Vossoughi, and N. Taghavinia, "Immobilization of TiO_2 on perlite granules for photocatalytic degradation of phenol," *Applied Catalysis B*, vol. 74, no. 1-2, pp. 53–62, 2007.

[42] K. Genov, I. Stambolova, M. Shipochka, I. Boevski, S. Vassilev, and V. Blaskov, "Ag coated bulgarian natural glass perlite via spray pyrolysis for decomposition of ozone," *Journal of the University of Chemical Technology & Metallurgy*, vol. 46, no. 4, pp. 363–368, 2011.

[43] Y.-H. Tseng, C.-S. Kuo, C.-H. Huang et al., "Visible-light-responsive nano-TiO_2 with mixed crystal lattice and its photocatalytic activity," *Nanotechnology*, vol. 17, no. 10, pp. 2490–2497, 2006.

[44] J. Yu, J. C. Yu, M. K.-P. Leung et al., "Effects of acidic and basic hydrolysis catalysts on the photocatalytic activity and microstructures of bimodal mesoporous titania," *Journal of Catalysis*, vol. 217, no. 1, pp. 69–78, 2003.

[45] "Fine ceramics (advanced ceramics, advanced technical ceramics)—test method for air-purification performance of semiconducting photocatalytic materials. Part 1: removal of nitric oxide," ISO/DIS 22197-1, 2007.

[46] V. Kalousek, J. Tschirch, D. Bahnemann, and J. Rathouský, "Mesoporous layers of TiO_2 as highly efficient photocatalysts for the purification of air," *Superlattices and Microstructures*, vol. 44, no. 4-5, pp. 506–513, 2008.

[47] Y. Ohko, Y. Nakamura, N. Negishi, S. Matsuzawa, and K. Takeuchi, "Photocatalytic oxidation of nitrogen monoxide using TiO_2 thin films under continuous UV light illumination," *Journal of Photochemistry and Photobiology A*, vol. 205, no. 1, pp. 28–33, 2009.

[48] A. Mitsionis, T. Vaimakis, C. Trapalis, N. Todorova, D. Bahnemann, and R. Dillert, "Hydroxyapatite/titanium dioxide nanocomposites for controlled photocatalytic NO oxidation," *Applied Catalysis B*, vol. 106, no. 3-4, pp. 398–404, 2011.

[49] T. Giannakopoulou, N. Todorova, G. Romanos et al., "Composite hydroxyapatite/TiO_2 materials for photocatalytic oxidation of NO_x," *Materials Science and Engineering B*, vol. 177, pp. 1046–1052, 2012.

[50] Y. K. Kho, W. Y. Teoh, L. Mädler, and R. Amal, "Dopant-free, polymorphic design of TiO_2 nanocrystals by flame aerosol synthesis," *Chemical Engineering Science*, vol. 66, no. 11, pp. 2409–2416, 2011.

[51] G. L. Chiarello, I. Rossetti, and L. Forni, "Flame-spray pyrolysis preparation of perovskites for methane catalytic combustion," *Journal of Catalysis*, vol. 236, no. 2, pp. 251–261, 2005.

[52] R. Strobel and S. E. Pratsinis, "Direct synthesis of maghemite, magnetite and wustite nanoparticles by flame spray pyrolysis," *Advanced Powder Technology*, vol. 20, no. 2, pp. 190–194, 2009.

[53] T. Ohsaka, F. Izumi, and Y. Fujiki, "Raman spectrum of anatase, TiO_2," *Journal of Raman Spectroscopy*, vol. 7, pp. 321–324, 1978.

[54] S. P. S. Porto, P. A. Fleury, and T. C. Damen, "Raman spectra of TiO_2, MgF_2, ZnF_2, FeF_2, and MnF_2," *Physical Review*, vol. 154, no. 2, pp. 522–526, 1967.

[55] F. Cerdeira, C. J. Buchenauer, F. H. Pollak, and M. Cardona, "Stress-induced shifts of first-order Raman frequencies of diamond- and zinc-blende-type semiconductors," *Physical Review B*, vol. 5, no. 2, pp. 580–593, 1972.

[56] B. G. Varshal, V. N. Denisov, B. N. Mavrin, G. A. Pavlova, V. B. Podobedov, and E. Kh. Sterin, "Spectra of combination and hypercombination scattering of light by glasses of the TiO_2-SiO_2 system," *Optics and Spectroscopy*, vol. 47, pp. 344–362, 1979.

[57] O. Carp, C. L. Huisman, and A. Reller, "Photoinduced reactivity of titanium dioxide," *Progress in Solid State Chemistry*, vol. 32, no. 1-2, pp. 33–177, 2004.